SINERGI Vol. 30, No. 2, June 2026: 319-336
http://publikasi.mercubuana.ac.id/index.php/sinergi
http://doi.org/10.22441/sinergi.2026.2.001

Texture features-based automated classification for dental caries level images

Yessi Jusman[1,*], Sartika Puspita[2], Nanang Kurniawan[1], Syahrul Gunawan[1], Berli Paripurna Kamiel[3], Zul Indra[4], Nor Ashidi Mat Isa[5]
[1]Department of Electrical Engineering Faculty of Engineering, Universitas Muhammadiyah Yogyakarta, Indonesia
[2]Department of Oral Biology, Dental School, Universitas Muhammadiyah Yogyakarta, Indonesia
[3]Department of Mechanical Engineering Faculty of Engineering, Universitas Muhammadiyah Yogyakarta, Indonesia
[4]Department of Computer Science, Universitas Riau, Indonesia
[5]School of Electrical and Electronic Engineering, Universiti Sains Malaysia, Malaysia

Abstract
Dental caries is a globally prevalent oral health issue posing substantial challenges regarding health outcomes and economic burden. Early detection is critical to prevent the progression of the disease and ensure effective treatment. This study aims to develop a machine learning-based system for classifying dental caries severity using X-ray radiographic images. The proposed system integrates two prominent feature extraction techniques: Histogram of Oriented Gradients (HOG) and Haar Wavelet Transform, applied at varying levels (HOG 50×50, HOG 70×70, Haar Level 1, and Haar Level 2) to capture both texture and frequency-based features. These extracted features are subsequently classified using two machine learning algorithms, Support Vector Machines (SVM) and k-Nearest Neighbors (KNN), across four models: Cubic SVM, Quadratic SVM, Weighted KNN, and Fine KNN. A dataset of 347 dental X-ray images was expanded to 1,388 through augmentation techniques and pre-processed into grayscale for consistency. The results unveiled that combining Haar Wavelet features with the KNN classifier yielded the highest classification accuracy, reaching 97.99% during training and an AUC of 0.99. These findings underscore the potential of combining advanced feature extraction methods with robust machine learning algorithms to enhance the precision of dental caries detection in clinical practice. This system presents a significant step forward in automating diagnostic procedures, providing a reliable and efficient tool for early caries detection, ultimately contributing to improved patient outcomes.

Keywords:
Dental Caries;
Features Extraction;
Machine Learning;

Article History:
Received: September 30, 2024
Revised: June 30, 2025
Accepted: August 29, 2025
Published: June 2, 2026

Corresponding Author:
Yessi Jusman
Department of Electrical Engineering, Universitas Muhammadiyah Yogyakarta, Indonesia
Email: yjusman@umy.ac.id

INTRODUCTION

Dental caries remains one of the most prevalent chronic conditions worldwide and continues to impose a significant burden on health systems through treatment costs, lost productivity, and reduced quality of life [1]. Globally, the WHO has reported that by 2022, untreated dental caries affected 2,029,495,070 individuals, making it one of the leading causes of oral disease burden. The economic impact of dental caries is substantial, with direct and indirect costs contributing to an annual expenditure of approximately US$387 billion in direct costs and US$323 billion in indirect costs. The highest prevalence of dental caries is in densely populated regions, particularly in South-East Asia and the Western Pacific. In

Indonesia specifically, there are an estimated 69,024,654 cases of dental caries in permanent teeth, representing 3.4% of the global caseload. Additionally, the country has approximately 38,105,664 cases of dental caries in deciduous teeth, accounting for 3.5% of the global total [2]. These statistics highlight the significant burden of dental caries both globally and in Indonesia, emphasizing the urgent need for effective oral health strategies and interventions.

Early detection and accurate characterization of carious lesions are essential to enable minimally invasive interventions and to prevent irreversible structural damage. Conventional diagnostics, visual-tactile inspection supplemented by bitewing, periapical, or panoramic radiography, have been widely utilized but can miss early, non-cavitated lesions and are subject to inter-observer variability and ionizing radiation exposure [3, 4, 5].

Digital imaging and artificial intelligence (AI) advances have catalyzed a transition from subjective assessments to quantitative, image-based decision support [6, 7, 8, 9, 10]. Modern pipelines pair image acquisition with preprocessing, segmentation [11, 12, 13], feature extraction, and supervised learning to detect and classify caries by location and severity. These pipelines promise greater reproducibility, sensitivity to subtle demineralization, and scalable screening workflows in both clinic and community settings.

Within this paradigm, machine learning (ML) and deep learning (DL) models have been applied to radiographs and alternative imaging modalities to automate lesion detection, boundary delineation, and risk stratification. Classical feature-based approaches (e.g., texture and shape descriptors) coexist with end-to-end convolutional neural networks (CNNs) learn hierarchical features directly from pixel data. Explainable AI techniques aim to improve clinical trust by highlighting image regions that drive model predictions [14][15].

Despite encouraging results, several barriers limit routine deployment. Data scarcity and inconsistent labeling standards hinder robust training and cross-site generalization [16, 17, 18, 19]; imaging artifacts and anatomical variability complicate segmentation and classification [20, 21, 22, 23, 24, 25, 26]; and cost or workflow constraints can impede adoption of advanced modalities. Hence, addressing these challenges is central to translating research prototypes into dependable preventive and restorative dentistry tools.

Early work in image-based caries classification relied on handcrafted features engineered to capture intensity, texture, and shape variations associated with demineralization. Common descriptors include Hu and Zernike moment invariants for shape [27, 28, 29], Gray Level Co-occurrence Matrix (GLCM) and Histogram of Oriented Gradients (HOG) for texture and edge structure, and simple first-order statistics. These features are typically fed to classical classifiers such as Support Vector Machines (SVM), K-Nearest Neighbors (KNN), and Multilayer Perceptron (MLP), achieving competitive accuracies on curated datasets and enabling interpretable decision boundaries [30][31].

The emergence of deep learning has shifted the field toward end-to-end representation learning. CNN architectures (e.g., AlexNet, GoogLeNet, ResNet-50) trained on dental radiographs have reported high diagnostic performance, while encoder–decoder models such as U-Net and its variants support pixel-wise segmentation of occlusal and approximal lesions. Ensemble strategies that aggregate multiple CNNs or combine CNNs with gradient-boosting or random-forest heads further improve robustness, particularly under class imbalance [32]. In parallel, explainability methods (Grad-CAM, saliency maps) provide visual rationales that clinicians can inspect.

Beyond X-ray imaging, several non-ionizing modalities have been developed to expand diagnostic capability, particularly for detecting early enamel lesions. Near-infrared (NIR) reflectance and hyperspectral imaging provide enhanced contrast between sound and demineralized tissues without exposing patients to radiation [33, 34, 35, 36]. Optical Coherence Tomography (OCT) offers high-resolution, depth-resolved cross-sections [37, 38, 39, 40, 41, 42]. Micro-CT serves as a high-resolution reference standard for in vitro studies, while emerging techniques such as photoacoustic imaging and terahertz spectroscopy are under investigation for non-destructive, depth-aware analysis [43, 44, 45, 46, 47]. However, their clinical adoption is constrained by operational complexity, specialized training requirements, and high costs, limiting routine use in primary care [41, 48, 49].

Image processing remains pivotal for reliable pipelines across modalities. Preprocessing steps (noise reduction, contrast enhancement, illumination correction) mitigate acquisition variability; segmentation strategies span thresholding, active contours, region growing, level sets, and CNN-based methods; and

post-processing refines lesion masks via morphological operations [4, 51, 52, 53, 54, 55]. For classical ML, feature selection (e.g., mutual information, recursive elimination) curbs overfitting and improves generalization. For DL, data augmentation, transfer learning, and fine-tuning from extensive natural-image backbones are routine to counter limited labeled data.

Clinically realistic datasets are heterogeneous in sensor type, exposure, and patient population, causing a domain shift that degrades model performance outside the training site. Annotating lesion boundaries is labor-intensive and subjective, particularly for approximal caries with ambiguous edges; weak or noisy labels can bias training. Imbalanced class distributions (few advanced lesions) complicate optimization and inflate apparent accuracy if not handled with calibrated metrics. Finally, deployment demands calibration, uncertainty estimation, and human-AI interaction design to prevent automation bias.

Recent trends address these gaps through self-supervised and semi-supervised learning to leverage unlabeled images; curriculum and active learning to prioritize informative samples for expert annotation; and domain adaptation or normalization to harmonize data across devices and clinics. Lightweight CNNs and on-device inference broaden primary care and tele-dentistry access, while multimodal fusion integrates complementary contrast mechanisms. Standardized benchmarks, reporting guidelines, and external validation across institutions are increasingly recognized as prerequisites for clinical translation.

Accordingly, clinically integrated systems will likely combine non-ionizing imaging for screening, radiography for confirmatory assessment, and AI for triage, severity grading, and progression monitoring. Incorporating longitudinal data, calibration to real-world prevalence, and explainability tailored to dental workflows can enhance trust and adoption. As datasets grow and evaluation protocols mature, image-based ML/DL methods are poised to support earlier, more precise caries management and to reduce overtreatment through evidence-guided prevention.

Radiographic imaging remains fundamental to caries diagnosis by enabling detailed visualization of dental and bony structures, although its accuracy is constrained by image quality variability, necessitating advanced imaging modalities and more reliable diagnostic tools.

To address these limitations, biomedical researchers have increasingly applied AI and image processing algorithms for dental caries. Although recent advancements in deep learning, particularly CNNs, have demonstrated remarkable success in learning complex and hierarchical representations directly from raw medical images, their effectiveness typically depends on access to large, annotated datasets and substantial computational resources. Given that this study's dataset consists of 1,388 images after augmentation, a traditional machine learning approach with handcrafted feature extraction was adopted to maintain model interpretability and reduce the risk of overfitting.

The development of machine learning applications in dentistry remains necessary to improve diagnostic accuracy and support clinical decision-making. This study offers a machine learning–based solution for classifying dental caries through a comparative analysis of feature extraction and classification techniques. Specifically, two feature extraction methods, Histogram of Oriented Gradients (HOG) and Haar wavelet, were examined at different levels (HOG 50×50, HOG 70×70, Haar 1, and Haar 2). The extracted features were subsequently classified using Support Vector Machine (SVM) and K-Nearest Neighbors (KNN) with selected models, including Cubic SVM, Quadratic SVM, Weighted KNN, and Fine KNN.

This study primarily seeks to identify the most effective combination of feature extraction and classification methods to obtain a more optimal model for image-based dental caries diagnosis, thereby supporting automated and precise decision-making in modern dentistry. The findings are expected to enhance early detection and clinical outcomes in dental healthcare.

METHOD

This study was designed to classify four levels of dental care. The classification was based on two feature extraction algorithms: HOG (using two cell sizes, 50×50 and 70×70) and Haar Wavelet (using two levels, 1 and 2). The classification methods were SVM (Cubic and Quadratic) and KNN (Weighted and Fine). Figure 1 illustrates the flowchart of the system design.

Data Acquisition

This study employed 347 X-ray radiographic images of patients with dental caries, obtained from the Dental and Oral Hospital of Universitas Muhammadiyah Yogyakarta.

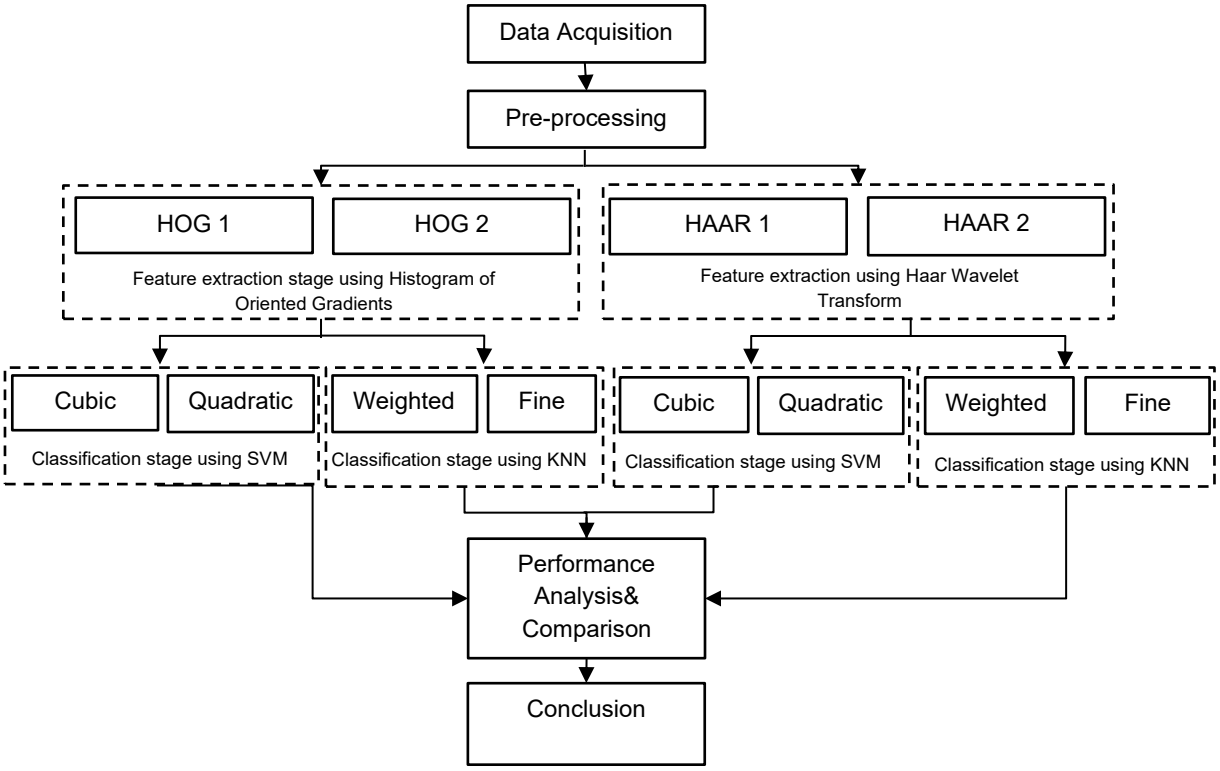

Figure 1. Flowchart of the System Design

All data ethically encoded to ensure confidentiality. The X-ray images were categorized into four classes based on the severity of the caries: 125 images of class 1 (mild caries), 94 images of class 2 (moderate caries), 80 images of class 3 (advanced caries), and 48 images of class 4 (severe caries).

This data variability was designed to develop an AI model capable of accurately detecting dental caries through image processing and feature extraction techniques, resulting in a more effective X-ray-based diagnostic system applicable widely in clinical practice. This class distribution reflects the natural imbalance often encountered in clinical datasets.

Pre-processing

During pre-processing, systematic steps were carried out to enhance the quality and variety of the image data for effective processing and classification. The initial step was data augmentation, where various flipping techniques were applied, including vertical, horizontal, and combined vertical-horizontal flips. This augmentation aimed to escalate the dataset's diversity without altering the original images' core characteristics, thereby improving the model's performance during training. After augmentation, the images remained in their original RGB format; hence, an RGB2Gray conversion was performed to transform them into grayscale. This step was essential to remove irrelevant color information and focus on the intensity values that were more appropriate for X-ray images.

Subsequently, the grayscale images were resized to a uniform resolution of 223x585 pixels. Standardizing the image resolution was crucial to address the varying resolutions of the original images, which could otherwise cause errors during feature extraction. As a result of this pre-processing pipeline, the dataset expanded to 1,388 images across four classes, with improved variation and image quality, expected to enhance the accuracy and effectiveness of the model in detecting dental caries. Figure 2 depicts the visualizations of the pre-processing stage.

Feature Extraction

Feature extraction on dental X-ray images, particularly for detecting dental caries, usually involves focusing on texture- and gradient-based characteristics [56]. This technique highlights minor differences in tooth structure that are often difficult to detect in raw X-ray images. This study experimented with two feature extraction techniques, each with two different levels. The HOG technique was applied at two levels of cell or block size, particularly 5050 (HOG 1) and 7070 (HOG 2).

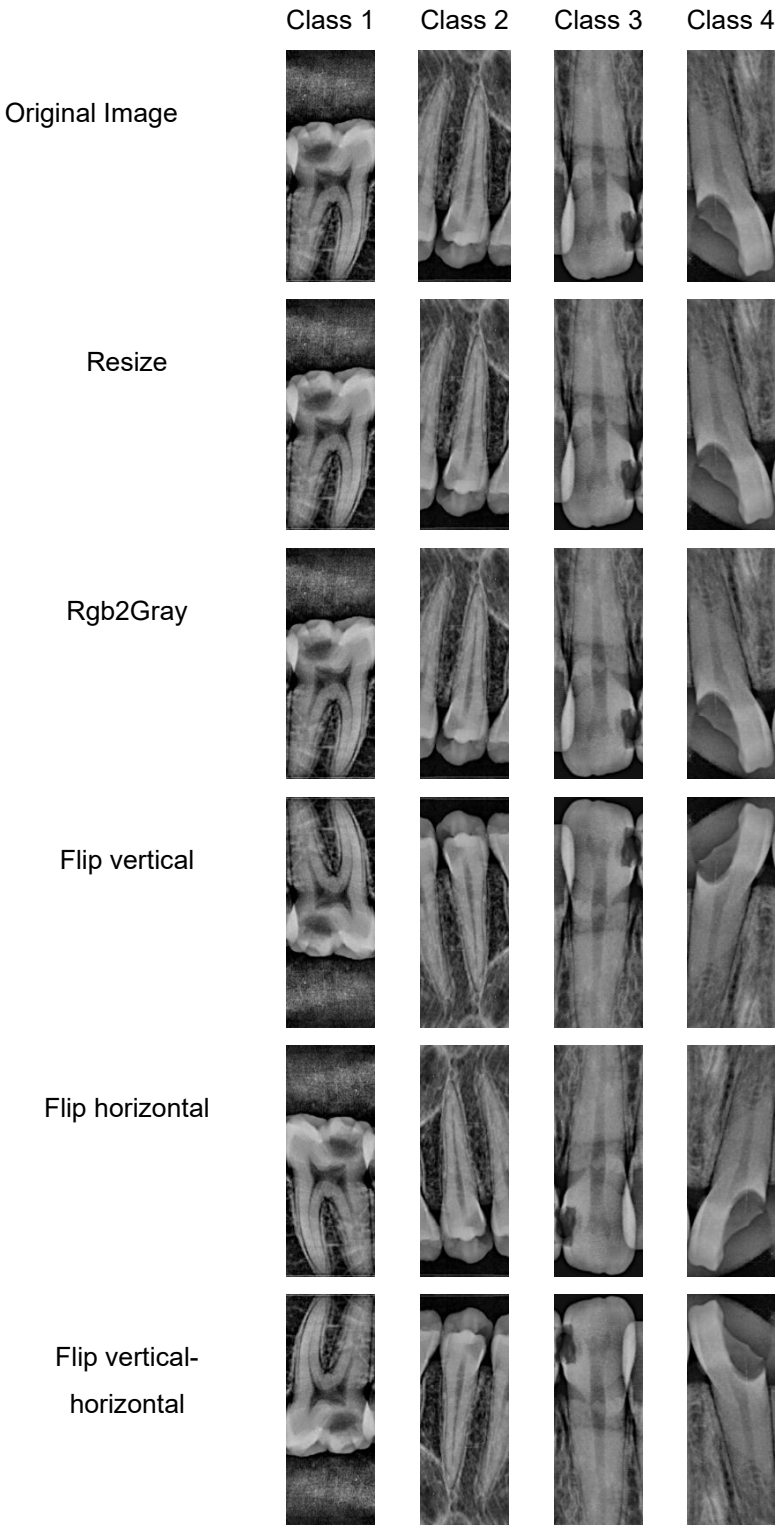

Figure 2. Pre-processing Stages

On the other hand, the Haar Wavelet technique was also implemented at two levels: Level 1 (HAAR 1) and Level 2 (HAAR 2). HOG has been widely adopted for capturing local gradient directions, making it highly effective for texture analysis in dental caries detection. HOG divides an image into connected small regions, computes the gradient or edge directions for each, and generates a histogram of these gradients [57].

It helps identify features like the borders of cavities, lesions, and other structural variations in the tooth. The HOG 50×50 and HOG 70×70 refer to cell sizes, indicating how the image is partitioned into cells for feature extraction, with 50×50 and 70×70 pixel cells. The gradients from these cells were aggregated to detect irregularities typical of caries. The intensity gradient at each pixel in the image was calculated using the Sobel filter. Equation (1) represents the gradient in the horizontal (Gx) and vertical (Gy) directions, while (2) denotes the magnitude ($|G|$) and orientation θ of the gradient [58].

$$G_x = \frac{\partial I}{\partial x}, \quad G_y = \frac{\partial I}{\partial y} \tag{1}$$

$$|G| = \sqrt{G_x^2 + G_y^2}, \quad \theta = \tan^{-1}\left(\frac{G_y}{G_x}\right) \tag{2}$$

Haar wavelet transform is another powerful method utilized in dental image analysis, known for capturing spatial and frequency information [59, 60, 61]. In this study, the Haar wavelet transform was employed as a feature extraction method and applied at Levels 1 and 2. Composing an image into wavelet coefficients allows for multi-resolution analysis, critical in identifying both large and small-scale patterns indicative of dental caries. Haar wavelet effectively detected fine texture variations and helped recognize early-stage caries, which might not be easily visible in standard X-ray images. The computation of the Haar wavelet is relatively easy [62]. The definition of the mother wavelet function ψ(t) is defined in (3).

$$\psi(t) = \begin{cases} 1 & 0 \le t < 0.5, \\ -1 & 0.5 \le t < 1, \\ 0 & \text{otherwise} \end{cases} \tag{3}$$

The scaling function (father wavelet) is provided in (4).

$$\phi(t) = \begin{cases} 1 & 0 \le t < 1, \\ 0 & \text{otherwise} \end{cases} \tag{4}$$

Classification

This study adopted two classification techniques to detect dental caries: SVM and KNN. Each method was further explored using specific models: Cubic SVM, Quadratic SVM, Weighted KNN, and Fine KNN. These methods were selected for their effectiveness in medical image classification, particularly in detecting subtle features in dental X-ray images. The classification was applied to the features extracted from the X-ray images using HOG: HOG 1 and HOG 2, and Haar wavelet transform: Haar Level 1 and Haar Level 2.

These feature extraction techniques helped capture essential spatial and frequency information, making the classification models more robust in distinguishing between carious and non-carious regions. By leveraging these extracted features, the classifiers could accurately process the input data and predict the class of each image, thereby assisting in the early detection and diagnosis of dental caries.

SVM, the supervised learning approach, was applied to binary and multi-class classification tasks. It determined the most optimal hyperplane with the most significant margin, dividing data points of various classes. The optimization problem for SVM is expressed in (5) and (6):

Objective Function (Primal Form):

$$\min_{\mathbf{w},b,\xi} \frac{1}{2}\|\mathbf{w}\|^2 + C\sum_{i=1}^{n}\xi_i \tag{5}$$

Subject to:

$$y_i(\mathbf{w}\cdot\mathbf{x}_i + b) \ge 1 - \xi_i, \quad \xi_i \ge 0 \tag{6}$$

Description:

- ***w*** is the weight vector
- *b* indicates the bias
- ξ_i depict slack variables for handling misclassification
- *C* represents the regularization parameter
- y_i denote the class labels (+1 or −1)

Two specific SVM models, Cubic and Quadratic, were utilized in this investigation. Cubic SVM employed a cubic kernel function, allowing the model to handle more complex relationships in the data by transforming the input space into a higher dimension. This kernel type is beneficial when linear separability is insufficient. On the other hand, Quadratic SVM applied a quadratic kernel function, providing a less complex decision boundary than the cubic kernel. It is useful when a slightly more flexible boundary is required than linear models, but without the c complexity of higher-order kernels.

KNN is a non-parametric method that classifies a data point based on the majority vote of its k nearest neighbors. The distance metric (commonly Euclidean) was employed to discover the closest neighbors [63] as in (7).

$$d(\mathbf{x}, \mathbf{x}_i) = \sqrt{\sum_{j=1}^{m} (x_j - x_{ij})^2} \quad (7)$$

Description:

- x is the test data point
- x_i signifies a training data point
- x_i and x_{ij} are feature values

Two models of KNN were utilized: Weighted KNN and Fine KNN. Weighted KNN assigned a weight to each neighbor based on its distance to the query point, allowing closer neighbors to have more influence on the classification decision. This approach improved accuracy, especially when dealing with imbalanced or noisy data. Meanwhile, Fine KNN adopted a finer granularity by considering fewer neighbors, typically leading to more precise classifications where class boundaries are closely packed.

RESULTS AND DISCUSSION

HOG calculated features by computing the orientation gradients of an image, followed by the construction of histograms representing the distribution of these gradients within each cell. This method captured the structural properties of the image, particularly emphasizing edge directions and intensity. The extracted feature vector consisted of values between 0 and 1, representing the relative presence of gradient orientations in each region. In this study, HOG 1 was computed using a cell size of 50×50, resulting in 1,080 features, as presented in Table 1. Meanwhile, HOG 2, using a cell size of 70×70, generated 504 features, as displayed in Table 2. The Haar Wavelet Transform, on the other hand, decomposed an image into its high-frequency (detail) and low-frequency (approximation) components over multiple levels. This multi-scale decomposition captured both local and global image information. This research applied Haar Wavelet at Levels 1 and 2, with each level producing six feature values, as depicted in Table 3 and Table 4.

The results presented in Table 1 provide a detailed comparison of texture feature extraction values across four different classes, allowing for an in-depth evaluation of the variations in each feature. The differences in mean values for each feature indicate varying degrees of separation between the classes. Feature 1 generated only minor variations between the classes, with Class 4 exhibiting the highest mean value (0.150) and Class 1 having the lowest (0.141), while the standard deviations remained consistent across all classes. Similarly, Features 2 and 3 displayed minimal differences, with Class 4 maintaining a slightly higher mean than the other classes. These consistent standard deviations across the classes for Features 1 through 3 suggest that, despite some variations, these features may not provide significant discriminatory power for classifying the data.

However, more significant differences became apparent as the study progressed through the features. Feature 5 possessed the highest variation, where Class 1 recorded a notably higher mean (0.201) compared to the lower mean in Class 3 (0.168). This pattern continued with Feature 10, where the mean values rose significantly from Class 1 (0.167) to Class 4 (0.187), demonstrating a more precise differentiation between the classes. These features are characterized by more pronounced mean values and standard deviation variations.

This increased variance suggests they may be more pivotal in distinguishing between the different caries of classes. The final feature (Feature 1,080) also exhibited similar trends, with Class 4 showing the highest mean (0.173) and Class 1 the lowest (0.161), though the differences were less substantial. Overall, features with higher variability, such as Features 5 and 10, may offer stronger predictive capabilities for classification tasks, whereas features with minimal variation were likely to be less influential.

Table 1. Texture Feature Extraction Results by HOG 1

Features	Class 1	Class 2	Class 3	Class 4
	Average ± St Dev			
1	0.141 ± 0.061	0.149 ± 0.061	0.144 ± 0.065	0.150 ± 0.060
2	0.129 ± 0.059	0.136 ± 0.058	0.132 ± 0.060	0.137 ± 0.057
3	0.130 ± 0.053	0.137 ± 0.053	0.128 ± 0.051	0.133 ± 0.051
4	0.155 ± 0.068	0.155 ± 0.062	0.138 ± 0.056	0.141 ± 0.056
5	0.201 ± 0.107	0.194 ± 0.095	0.168 ± 0.064	0.171 ± 0.059
6	0.157 ± 0.065	0.158 ± 0.060	0.162 ± 0.062	0.163 ± 0.063
7	0.132 ± 0.053	0.140 ± 0.054	0.158 ± 0.057	0.161 ± 0.056
8	0.129 ± 0.057	0.143 ± 0.060	0.155 ± 0.059	0.157 ± 0.058
…	… ± …	… ± …	… ± …	… ± …
1080	0.161 ± 0.059	0.164 ± 0.065	0.167 ± 0.055	0.173 ± 0.054

Table 2. Texture Feature Extraction Results by HOG 2

Features	Class 1	Class 2	Class 3	Class 4
	Average ± St Dev			
1	0.144 ± 0.060	0.151 ± 0.058	0.155 ± 0.057	0.164 ± 0.052
2	0.134 ± 0.060	0.139 ± 0.056	0.141 ± 0.052	0.147 ± 0.048
3	0.131 ± 0.052	0.134 ± 0.050	0.134 ± 0.042	0.139 ± 0.044
4	0.149 ± 0.059	0.148 ± 0.053	0.143 ± 0.045	0.145 ± 0.050
5	0.191 ± 0.100	0.181 ± 0.078	0.171 ± 0.051	0.169 ± 0.051
6	0.151 ± 0.057	0.154 ± 0.052	0.167 ± 0.050	0.167 ± 0.052
7	0.134 ± 0.051	0.143 ± 0.050	0.163 ± 0.048	0.162 ± 0.048
8	0.135 ± 0.058	0.147 ± 0.058	0.164 ± 0.050	0.163 ± 0.050
…	… ± …	… ± …	… ± …	… ± …
504	0.162 ± 0.056	0.167 ± 0.061	0.173 ± 0.049	0.177 ± 0.049

Table 3. Texture Feature Extraction Results by Haar Level 1

Features	Class 1	Class 2	Class 3	Class 4
	Average ± St Dev			
Eh	0.465 ± 0.133	0.412 ± 0.105	0.331 ± 0.076	0.280 ± 0.098
Ev	0.118 ± 0.035	0.113 ± 0.035	0.077 ± 0.022	0.068 ± 0.025
Ed	0.030 ± 0.012	0.025 ± 0.011	0.020 ± 0.008	0.015 ± 0.007
stdCh	17.400 ± 3.220	16.800 ± 2.260	15.100 ± 1.550	14.100 ± 2.320
stdCv	8.750 ± 1.650	8.780 ± 1.420	7.260 ± 0.968	6.910 ± 1.130
stdCd	4.380 ± 1.010	4.070 ± 0.943	3.620 ± 0.669	3.250 ± 0.705

Table 4. Texture Feature Extraction Results by Haar Level 2

Features	Class 1	Class 2	Class 3	Class 4
	Average ± St Dev			
Eh	0.901 ± 0.244	0.412 ± 0.105	0.331 ± 0.076	0.280 ± 0.098
Ev	0.227 ± 0.056	0.113 ± 0.035	0.077 ± 0.022	0.068 ± 0.025
Ed	0.083 ± 0.028	0.025 ± 0.011	0.020 ± 0.008	0.015 ± 0.007
stdCh	48.200 ± 8.670	16.800 ± 2.260	15.100 ± 1.550	14.100 ± 2.320
stdCv	24.300 ± 3.980	8.780 ± 1.420	7.260 ± 0.968	6.910 ± 1.130
stdCd	14.600 ± 2.990	4.070 ± 0.943	3.620 ± 0.669	3.250 ± 0.705

The analysis of texture feature extraction results revealed critical insights into the effectiveness of various features for classifying dental caries based on X-ray images. The HOG method applied to these images produced varying degrees of separability across the four classes of dental caries. Specifically, comparing feature values (mean ± standard deviation) across the classes demonstrated that some features provided more significant differentiation, while others depicted minimal variation. This observation is crucial for determining which features hold the most discriminative power in the classification.

Features 5 and 10 exhibited substantial differences in mean values between the classes, with Class 1 consistently showcasing higher values than the other classes. These features depicted high variability (standard deviation) in Class 1, indicating that these texture features could capture critical details regarding the structural differences in dental caries severity. The higher variability suggests that Class 1 may encompass a broader range of caries severities or dental textures. Conversely, Features 2 and 3 displayed minor differences, with relatively small standard deviations, suggesting that these features did not contribute substantially to the differentiation between caries classes. This outcome aligns with previous research identifying certain texture features as more informative for medical image analysis, particularly in differentiating between subtle variations in tissue or structural anomalies [64].

The texture feature extraction results using HOG 2, presented in Table 2, highlight varying degrees of class separability across the four dental caries classes. Features 1 to 3 portrayed limited differentiation between the classes, with slight differences in mean values and low variability (standard deviation). In Feature 1, Class 4 generated the highest mean (0.164 ± 0.052), while Class 1 had the lowest (0.144 ± 0.060), but the overall variation across all classes was minimal. Similarly, Features 2 and 3 exhibited marginal differences in mean values, suggesting that these features may not significantly contribute to distinguishing between caries classes.

Features 5 and 10 demonstrated more substantial variations, signifying their potential to enhance class separability. Feature 5 identified a notable difference between Class 1 (0.191 ± 0.100) and Class 4 (0.169 ± 0.051), with a higher

standard deviation in Class 1, suggesting greater variability in this class.

Feature 10 further amplified this trend, with Class 4 having the highest mean (0.195 ± 0.043) and Class 1 the lowest (0.172 ± 0.058), signifying that this feature is particularly useful for distinguishing between the classes. These results suggest that while early features offer limited separation, later features, such as Features 5 and 10, have been more effective in improving classification accuracy in dental caries detection.

The analysis of texture features extracted using the HOG 2 method across different dental caries classes revealed insights into how these features have contributed to classification. From the presented results, Features 1 to 3 demonstrated minimal variability between classes, indicating limited effectiveness in distinguishing different severities of dental caries. It is consistent with findings from other medical imaging studies showing that early features in gradient-based extraction, like HOG, may not always capture sufficient detail for robust classification, especially when subtle variations between classes [65][66].

However, Features 5 and 10 presented notable differences in their mean values, with Class 1 generating significantly higher values than the other classes. It suggests that these features could capture more critical texture details, potentially related to the structural changes in caries progression, aligning with previous research on the effectiveness of HOG in medical image classification. Studies, such as those conducted by Jia et al., indicate that using HOG with advanced classifiers like SVM could significantly escalate accuracy in medical diagnosis by capturing more intricate edge and gradient information from the images [57].

The results from Table 3 demonstrate notable differences in the texture features extracted using Haar Level 1 across the four dental caries classes. Eh, Ev, and Ed consistently depicted decreasing values from Class 1 to Class 4, with Class 1 exhibiting the highest mean values across these features. Eh ranged from 0.465 ± 0.133 in Class 1 to 0.280 ± 0.098 in Class 4, indicating a clear differentiation between the classes. Similarly, Ev and Ed followed this trend, reflecting their ability to capture structural variations in the dental X-ray images. These results imply that these features were particularly effective in distinguishing between higher and lower severity levels of dental caries.

Several features, particularly stdCh, stdCv, and stdCd, further supported this differentiation, with Class 1 consistently showing higher mean values than Class 4. stdCh yielded a mean of 17.400 ± 3.220 in Class 1, while Class 4 recorded 14.100 ± 2.320, implying greater variability in texture in the higher classes. The similar patterns observed in stdCv and stdCd reinforced the importance of these features in class separation. Overall, the extracted features could provide a strong foundation for distinguishing between the different severity levels of dental caries, with clear separability between Class 1 and Class 4, supporting their adoption in machine learning models for automated classification. Analyzing the texture features extracted using Haar Level 1 revealed essential insights into their role in distinguishing between different dental caries classes. Features such as Eh, Ev, and Ed depicted a consistent decline in mean values from Class 1 to Class 4, suggesting that these features could capture critical structural differences in dental X-ray images. Specifically, Eh demonstrated the highest variation between the classes, with Class 1 exhibiting a mean of 0.465 ± 0.133, while Class 4 produced a significantly lower value of 0.280 ± 0.098. This variation indicates that Eh effectively captured texture changes related to caries severity, making it a valuable feature for classification. Studies have unveiled that wavelet-based features like Eh are crucial in identifying texture variations in medical [59], [60].

StdCh, stdCv, and stdCd also disclosed notable differences across the classes, particularly in Class 1, which consistently exhibited higher mean values than Class 4. stdCh in Class 1 (17.400 ± 3.220) was substantially higher than in Class 4 (14.100 ± 2.320), indicating that horizontal texture variation was more pronounced in more severe caries cases. This trend continued with stdCv and stdCd, highlighting the significance of standard deviation-based features in capturing subtle texture variations.

The results presented in Table 4 highlight significant differences in the texture features extracted using Haar Level 2 across the four dental caries classes. Eh demonstrated the most pronounced variation, with Class 1 displaying the highest mean value (0.901 ± 0.244) and Class 4 the lowest (0.280 ± 0.098). Similarly, Ev and Ed consistently declined in mean values from Class 1 to Class 4, suggesting that these features effectively captured the structural variations in the X-ray images. This pattern underscores that Eh, Ev, and Ed were useful in distinguishing between classes, especially Class 1 and 4.

Table 4 discloses that Haar Level 2 features captured meaningful distinctions across the four dental caries classes. Features such as Eh, Ev, and Ed consistently declined from Class 1 to Class 4, with Eh ranging from 0.901 ± 0.244 (Class 1) to 0.280 ± 0.098 (Class 4), indicating strong discriminative capacity.

Similarly, stdCh, stdCv, and stdCd followed the same pattern, reinforcing their relevance for class separation. stdCh decreased markedly from 48.200 ± 8.670 (Class 1) to 14.100 ± 2.320 (Class 4). These trends signify that structural degradation associated with caries progression could be well-captured by Haar-derived features.

These findings align with prior studies emphasizing texture- and frequency-based descriptors for medical image classification [60][67] where gradient and edge patterns have proven effective in identifying pathological changes. The consistent separability, particularly between early (Class 1) and advanced stages (Class 4), highlights the suitability of Haar Level 2 features for enhancing multi-class caries detection.

The texture features extracted using Haar Level 2 demonstrated strong potential for improving dental caries classification. The consistent differences observed between Class 1 and Class 4 across multiple features, particularly Eh, stdCh, and stdCv, signify that these features could effectively capture critical variations in the X-ray images.

Table 5 presents the classification accuracy for various machine learning models applied to X-ray dental caries classification, including SVM (Cubic and Quadratic) and K-NN (Weighted and Fine). These models utilized different feature extraction algorithms, i.e., HOG 1, HOG 2, Haar Wavelet Level 1, and Level 2. These models were evaluated over ten runs, with the average accuracy and standard deviation provided for each combination of classifier and feature extraction method.

The results of the HOG 1 and HOG 2 features revealed that Cubic SVM consistently outperformed Quadratic SVM, achieving an average accuracy of 75.28% for HOG 1 and 77.60% for HOG 2. This outcome suggests that the cubic kernel could better capture the underlying patterns in the dental X-ray images, particularly when utilizing a higher feature extraction level, such as HOG 2. On the other hand, the K-NN classifiers, particularly Weighted K-NN, exhibited lower performance when paired with the HOG features, with average accuracies of 71.09% for HOG 1 and 72.21% for HOG 2. It implies that, although HOG provided informative features, the complexity inherent in dental X-ray images required a classifier to model nonlinear decision boundaries effectively, which the SVM appeared to handle better than K-NN.

The comparative training results using Haar Wavelet features at Level 1 and 2 revealed clear performance trends across SVM and K-NN classifiers (Table 5). The analysis uncovered that the depth of wavelet decomposition and the choice of classification algorithm significantly affected the accuracy and stability of dental caries classification models.

For Haar Level 1, the highest training accuracy was achieved using the Fine K-NN classifier, with an average of 94.80% (±0.47), followed by Weighted K-NN at 93.34% (±1.17). In contrast, the SVM classifiers with Cubic and Quadratic kernels yielded considerably lower accuracies, 77.19% and 66.65%, respectively, with slightly higher variability. It indicates that the textural features extracted at Level 1 were more effectively exploited by non-parametric classifiers like K-NN, sensitive to localized patterns, than SVM, which relies on global decision boundaries. A similar trend was observed for Haar Level 2, where K-NN again outperformed SVM by a wide margin. Fine K-NN reached the highest overall training accuracy of 97.99% (±0.58), while Weighted K-NN achieved 96.65% (±0.56). Although SVM classifiers improved performance with Haar Level 2 features, rising to 81.39% (Cubic) and 76.30% (Quadratic), they still lagged the K-NN models in accuracy and consistency.

These results strongly hint that Haar Level 1 and 2 features were more compatible with K-NN classifiers. The localized nature of K-NN allows it to take better advantage of detailed texture variations captured by Haar decomposition, especially at deeper levels. In contrast, SVM classifiers may struggle with handcrafted features, particularly in multi-class classification tasks, unless further tuning or kernel optimization is applied.

In conclusion, integrating Haar wavelet-based features with K-NN classifiers offered a more effective and stable solution for dental caries classification from radiographic images. It highlights the significance of aligning feature characteristics with classifier architecture to maximize diagnostic accuracy and robustness.

These findings advocate for a strategic alignment of feature extraction depth and classifier capabilities to maximize the diagnostic potential of machine learning models in healthcare applications, ultimately contributing to more effective and reliable caries detection.

Table 5. Comparison of Training Results for HOG and Haar Wavelet Features

Run	HOG 1				HOG 2				Haar 1				Haar 2			
	SVM		K-NN		SVM		K-NN		SVM		K-NN		SVM		K-NN	
	Cubic	Quadratic	Weighted	Fine	Cubic	Quadratic	Weighted	Fine	Cubic	Quadratic	Weighted	Fine	Cubic	Quadratic	Weighted	Fine
	Accuracy (%)															
1	75.7	73.9	71.2	73.4	77.3	76.6	72.0	73.7	78.0	67.5	92.3	94.5	80.7	76.2	96.5	96.8
2	75.1	74.0	71.6	**74.9**	77.8	76.1	72.5	74.1	**78.4**	**67.9**	93.3	95.1	80.3	75.9	95.9	**98.6**
3	74.1	72.9	71.3	74.3	77.5	75.7	72.5	74.5	75.9	67.0	92.9	94.2	81.8	76.4	96.9	98.4
4	**76.2**	72.9	71.0	74.4	**77.9**	**76.7**	73.0	74.7	77.1	66.5	93.8	94.4	81.6	**77.1**	95.8	97.8
5	74.8	72.6	70.9	74.3	78.1	75.7	72.3	73.4	76.0	66.0	**95.9**	94.8	81.7	75.9	97.0	97.9
6	75.6	74.0	69.7	74.7	77.8	76.4	**73.3**	**75.3**	77.1	65.7	91.9	94.4	82.3	76.9	96.0	97.9
7	75.4	73.1	71.3	73.3	77.1	76.3	70.9	74.1	77.9	66.3	94.4	95.1	**82.5**	76.6	**97.4**	97.3
8	75.6	**74.3**	70.7	73.9	78.1	76.3	72.0	74.4	77.1	67.0	92.3	**95.8**	81.3	75.9	97.0	98.3
9	75.3	74.2	71.5	74.5	77.5	76.2	71.8	74.5	77.0	66.8	93.3	95.0	81.1	75.4	97.1	98.3
10	75.0	73.7	**71.7**	74.4	76.9	75.5	71.8	73.4	77.4	65.8	93.3	94.7	80.6	76.7	96.9	98.6
Ave	**75.28**	**73.56**	**71.09**	**74.21**	**77.60**	**76.15**	**72.21**	**74.21**	**77.19**	**66.65**	**93.34**	**94.80**	**81.39**	**76.30**	**96.65**	**97.99**
St Dev	**0.58**	**0.62**	**0.58**	**0.52**	**0.41**	**0.40**	**0.68**	**0.60**	**0.80**	**0.73**	**1.17**	**0.47**	**0.73**	**0.53**	**0.56**	**0.58**

The testing results presented in Table 6 and Table 7 illustrate the comparative performance of various classification models using HOG and Haar wavelet feature extraction methods on different levels of dental caries severity. The metrics employed for evaluation included accuracy, precision, recall, specificity, and F1-score, providing a holistic overview of the performance of each model at multiple levels.

The comparative evaluation of HOG and Haar Wavelet Transform features revealed a consistent performance advantage favoring Haar-based descriptors across all classification models. While HOG 1 and HOG 2 features achieved moderate accuracy, ranging from 71% to 77%, Haar features, notably Haar Level 1, demonstrated superior classification capability, attaining the highest accuracy of 87.88% with the Weighted KNN classifier. This significant difference could be attributed to Haar's multi-resolution analysis, which effectively captured local and global texture variations, making it more suitable for detecting the nuanced structural changes in dental radiographic images. In contrast, HOG features emphasize edge orientation, which may not fully represent the frequency-based characteristics crucial in identifying early and advanced caries.

The testing performance of HOG Level 1 and Level 2 features indicates that SVM classifiers consistently outperformed K-NN in accuracy and stability. For HOG Level 1, Quadratic SVM achieved the highest accuracy of 77.09% ± 3.15, with balanced precision (74.85%) and recall (74.88%), while Cubic SVM produced similar results with slightly lower variability.

In contrast, Weighted KNN generated the lowest accuracy (71.67% ± 6.13) and F1-score (62.31% ± 7.23), indicating poor and unstable classification. Although Fine KNN achieved a comparable accuracy of 77.15%, its precision and recall were lower than those of SVM. A similar trend was observed for HOG Level 2, where Quadratic SVM attained the most outstanding overall performance with 77.55% ± 1.42 accuracy and the highest specificity (80.34%), followed by Cubic SVM with an F1-score of 76.11%. K-NN models again performed less effectively, with Weighted KNN recording low recall and unstable specificity (0.77 ± 0.11). These results suggest that SVM models could generalize more from HOG-based features representing global gradient orientation patterns. At the same time, K-NN was more sensitive to local noise and less effective in capturing meaningful texture variation in radiographic data. Thus, SVM was the preferred classifier for HOG feature-based dental caries classification.

The results from Haar Level 1 and 2 feature extraction highlight the strong performance of frequency-based features in enhancing classification accuracy. Weighted K-NN with Haar Level 1 acquired the highest average accuracy (87.88%) and specificity (90.72%), indicating its effectiveness in distinguishing caries from non-caries cases. Quadratic SVM also depicted robust performance across both Haar levels, with an accuracy of 81.81% for Level 1 and 84.23% for Level 2, supported by high recall and specificity. These findings underscore the discriminative strength of Haar features in supporting reliable caries classification across varying severity levels.

Table 6. Classification Testing Performance using HOG Features

Feature Types	Classifier	Accuracy (%)	Precision (%)	Recall (%)	Specificity (%)	F1-score (%)
HOG 1	Cubic SVM	77.04 ± 2.14	74.15 ± 3.84	74.37 ± 6.12	79.47 ± 3.26	74.05 ± 2.32
HOG 1	Quadratic SVM	77.09 ± 3.15	74.85 ± 5.91	74.88 ± 5.93	79.27 ± 5.12	74.62 ± 3.38
HOG 1	Fine KNN	77.15 ± 4.07	74.77 ± 9.16	74.67 ± 8.33	79.87 ± 7.61	74.19 ± 4.42
HOG 1	Weighted KNN	71.67 ± 6.13	64.74 ± 16.33	63.09 ± 10.54	78.34 ± 11.72	62.31 ± 7.23
HOG 2	Cubic SVM	77.17 ± 4.21	76.05 ± 3.41	76.87 ± 9.22	78.07 ± 3.21	76.11 ± 4.34
HOG 2	Quadratic SVM	77.55 ± 1.42	73.90 ± 2.29	74.06 ± 4.61	80.34 ± 1.87	73.87 ± 1.57
HOG 2	Fine KNN	75.05 ± 5.29	71.69 ± 9.38	71.67 ± 8.99	78.31 ± 7.65	71.17 ± 5.83
HOG 2	Weighted KNN	72.69 ± 4.49	70.38 ± 12.45	69.16 ± 6.37	0.77 ± 0.11	69.00 ± 4.83

Table 7. Classification Testing Performance using Haar Wavelet Features

Feature Types	Classifier	Accuracy (%)	Precision (%)	Recall (%)	Specificity (%)	F1-score (%)
Haar 1	Cubic SVM	79.70 ± 2.25	74.29 ± 18.18	72.69 ± 18.95	85.93 ± 10.28	70.53 ± 2.88
Haar 1	Quadratic SVM	81.81 ± 7.79	74.58 ± 18.16	77.49 ± 14.51	85.43 ± 10.84	74.43 ± 10.07
Haar 1	Fine KNN	85.90 ± 1.05	81.76 ± 11.50	79.77 ± 14.09	90.38 ± 6.92	79.30 ± 1.42
Haar 1	Weighted KNN	87.88 ± 3.45	82.85 ± 11.96	84.38 ± 12.76	90.72 ± 7.13	82.37 ± 4.79
Haar 2	Cubic SVM	81.13 ± 2.79	76.01 ± 13.33	77.77 ± 15.48	85.09 ± 9.54	74.97 ± 3.45
Haar 2	Quadratic SVM	84.23 ± 1.58	77.96 ± 13.76	82.06 ± 10.30	86.63 ± 8.67	78.61 ± 1.99
Haar 2	Fine KNN	82.00 ± 3.45	75.78 ± 12.54	76.06 ± 14.38	86.68 ± 8.01	74.27 ± 4.56
Haar 2	Weighted KNN	82.17 ± 4.75	74.59 ± 14.27	76.74 ± 16.98	87.07 ± 8.55	72.80 ± 6.70

The clinical implications of these findings are substantial. In particular, the combination of Haar Level 1 features with the Weighted KNN classifier not only offered the highest classification accuracy but also balanced sensitivity (84.38%) and specificity (90.72%), which is critical for minimizing both false negatives and false positives in medical diagnosis. This level of performance implies strong potential for clinical deployment, especially in supporting general dentists in identifying severe caries cases that require urgent intervention. Haar features also exhibited higher recall, specificity, and F1-score across most models, suggesting better class discrimination and robustness. This superior performance was likely due to Haar's ability to capture localized frequency patterns, making it more effective than HOG for medical image textures. Overall, when optimized with Haar-based features, the proposed system could serve as a practical assistive tool in early caries detection, offering reliability, interpretability, and real-world applicability.

The analysis of Area Under Curve (AUC) values provided critical insight into the effectiveness of the proposed feature extraction methods and classifiers for dental caries detection, presented in Table 8. The AUC values approached 1, as observed consistently with Haar Level 1 and 2 features across multiple models, including Cubic SVM and Quadratic SVM. Weighted and Fine K-NN depicted excellent discriminatory capability between the four caries cases. These results demonstrated that Haar features effectively captured relevant and fine-grained features from dental X-ray images, enabling high classification accuracy and precise risk stratification of caries severity levels.

A high AUC reflects the model's ability to balance true positive rate (TPR) and false positive rate (FPR), essential for reducing misdiagnosis in clinical settings. Classifiers paired with texture information extracted by Haar wavelet achieved AUC values approaching 1.0, underscoring their effectiveness in balancing true positive and false positive rates, supporting early and accurate caries detection, and are an essential requirement for clinical diagnostic applications.

Several previous studies have explored the classification of dental caries using various machine learning and deep learning techniques, often with varying dataset sizes and class structures [67]. From a critical perspective (Table 9), while the study by Geetha et al. achieved the highest classification accuracy (97.1%) and an AUC of 0.98, its reliability is limited by the relatively small dataset (105 images) and binary class setting, which inherently simplifies the classification task and raises concerns of overfitting [31].

Lee et al. applied a multi-class approach for three caries progression categories, but performance was limited by a small dataset of only 50 images [67], resulting in 83.25% sensitivity and a 79.46% F1-score. In contrast, Imak et al. showed that deep learning models trained on a larger dataset of 340 images with two classes achieved up to 96.19% accuracy, highlighting the importance of sufficient data volume for better model performance [5].

Table 8. Comparison of Area Under Curve Classification Results

	HOG 1	HOG 2	Haar 1	Haar 2
Cubic SVM	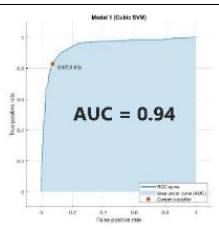	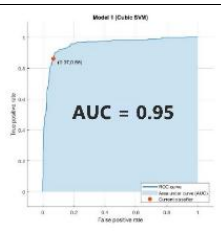	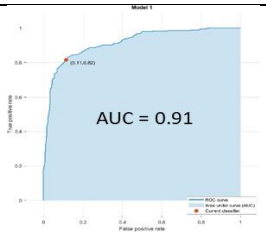	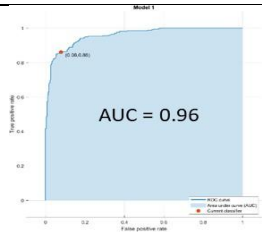
Quadratic SVM	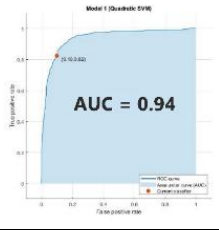	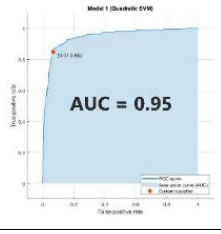	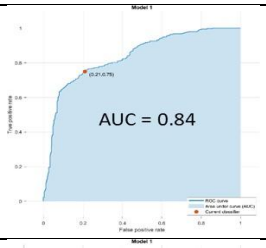	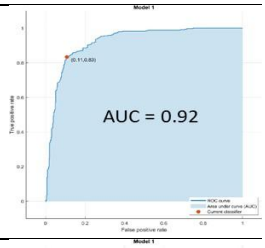
Weighted KNN	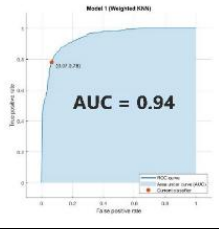	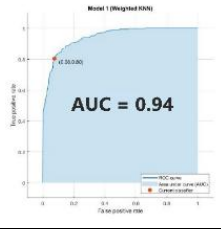	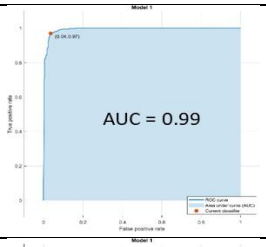	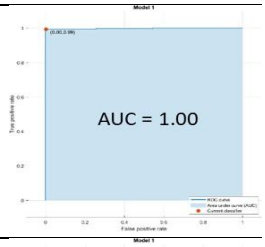
Fine KNN	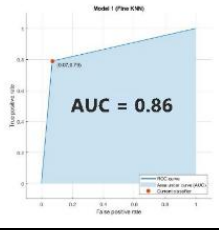	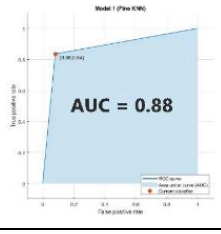	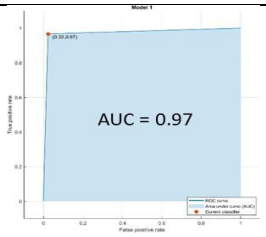	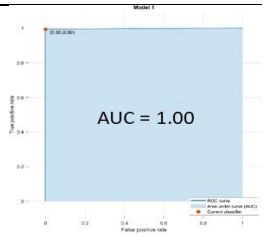

Table 9. Comparison of Previous Dental Caries Classification Results

Study/Author	Dataset	Method	Performance Metric
Geetha et al. (2020) [31]	105 images (intraoral) Two classes (normal and caries)	Statistical feature extraction and Neural Network	Accuracy of 97.1% and ROC area of 0.98
Lee et al. (2021) [67]	50 images (periapical) Three classes (initial, moderate, and extensive)	U-Net for caries segmentation and U-Net for structure segmentation CNN model	Sensitivity of 83.25% and F1 Score of 79.46%
Imak et al. (2022) [5]	340 images (periapical) Two classes (Caries and non-Caries)	Multi-Input deep CNN ensemble (MI-DCNNE) with Softmax layers SqueezeNet model Xception model	Accuracy of 96.19% 86.28% 80.25%
This study	347 images (periapical) Four classes (I, II, III, and IV)	Combination Haar Level 1 Wavelet and Weighted KNN models	Sensitivity Specificity of 84.38% and 90.72% Accuracy of 88% ROC area of 0.99

In contrast, the present study stands out for its balanced and realistic performance across multiple metrics. Utilizing the most extensive dataset (347 periapical images) and the most complex classification scheme (four caries classes), it attained a commendable accuracy of 88%, sensitivity of 84.38%, specificity of 90.72%, and an outstanding AUC of 0.99. The results indicate the effectiveness of the proposed approach, combining robust feature extraction techniques (Haar Wavelet Transform) and well-established classifiers (KNN). The comparative

advantage lies in the model's ability to balance complexity and performance using interpretable, computationally efficient methods suitable for clinical applications where computational resources may be constrained.

The findings confirmed that features derived from Haar wavelets provided a reliable and scalable foundation for dental caries detection when paired with classical machine learning models such as SVM and K-NN. Nonetheless, while these models offered strong quantitative performance, their interpretability remained limited compared to deep learning-based systems. Traditional machine learning models lacked the intuitive visual interpretability of modern deep learning methods. Although Haar and HOG features were explainable to a certain degree, they did not directly visualize the decision-making. Hence, future work should integrate visualization tools such as saliency maps or Gradient-weighted Class Activation Mapping (Grad-CAM) to bridge this interpretability gap and enhance the clinical transparency of the system.

CONCLUSION

This study presented a machine learning-based approach for classifying the severity of dental caries using periapical X-ray images. The system effectively differentiated between four caries stages by combining texture-based features, extracted through HOG and Haar Wavelet Transform, with SVM and K-NN classifiers. The best training performance was achieved using Haar features with Fine KNN (97.99%), while the most reliable testing result was obtained from Haar features with Weighted KNN, reaching 88% accuracy, 84.38% sensitivity, 90.72% specificity, and an AUC of 0.99. These findings demonstrated that Haar Wavelet features, particularly at lower decomposition levels, provided strong discriminative power when paired with distance-based classifiers like K-NN.

The results confirmed the potential of the proposed method for supporting early and accurate detection of dental caries. Its strong generalization performance highlights its suitability for clinical decision-support applications. Future work should explore hybrid models integrating handcrafted features with deep learning architectures to enhance diagnostic robustness and adaptability to larger, more diverse datasets.

ACKNOWLEDGMENT

The authors would like to thank the dentist and technologist in Dental and Oral Hospital (RSGM) of Universitas Muhammadiyah Yogyakarta, Pakuncen, Wirobrajan, Yogyakarta, Special Region of Yogyakarta, for providing primary data and information during this research study.

This research was supported by the Ministry of Research and Technology of the Republic of Indonesia through a research grant (0609.7/LL5-INT / AL.04 /2024).

REFERENCES

[1] R. Macey, T. Walsh, P. Riley, A.-M. Glenny, H. V. Worthington, L. O'Malley, J. E. Clarkson, and D. Ricketts, "Visual or visual-tactile examination to detect and inform the diagnosis of enamel caries," *Cochrane Database of Systematic Reviews*, vol. 6, Art. no. CD014546, 2021, doi: 10.1002/14651858.CD014546.

[2] N. Jain, U. Dutt, I. Radenkov, and S. Jain, "WHO's global oral health status report 2022: Actions, discussion and implementation," *Oral Diseases*, vol. 30, no. 2, pp. 73–79, Mar. 2024, doi: 10.1111/odi.14516.

[3] S. Valizadeh, M. Goodini, S. Ehsani, H. Mohseni, F. Azimi, H. Bakhshandeh, "Designing of a computer software for detection of approximal caries in posterior teeth," *Iranian Journal of Radiology*, vol. 12, no. 4, e16242, 2015, doi: 10.5812/iranjradiol.12(2)2015.16242.

[4] G. Vimalarani and U. Ramachandraiah, "Automatic diagnosis and detection of dental caries in bitewing radiographs using pervasive deep gradient based LeNet classifier model," *Microprocessors and Microsystems*, vol. 94, p. 104654, 2022, doi: 10.1016/j.micpro.2022.104654.

[5] A. Imak, A. Celebi, K. Siddique, M. Turkoglu, A. Sengur, and I. Salam, "Dental caries detection using score-based multi-input deep convolutional neural network," *IEEE Access*, vol. 10, pp. 18320–18329, 2022, doi: 10.1109/ACCESS.2022.3150358.

[6] W. Ahmed, A. Azhari, K. Fawaz, H. Ahmed, Z. Alsadah, A. Majumdar, R. Carvalho, "Artificial intelligence in the detection and classification of dental caries," *Journal of Prosthetic Dentistry*, vol. 133, no. 5, pp. 1326–1332, 2025, doi: 10.1016/j.prosdent.2023.07.013.

[7] Y. Liu, K. Xia, Y. Cen, S. Ying, Z. Zhao, "Artificial intelligence for caries detection: A novel diagnostic tool using deep learning algorithms," *Oral Radiology*, vol. 40, pp. 375–384, doi: 10.1007/s11282-024-00741-x.

[8] M. Rahmanzadeh, A. Rustamzadeh, E. A. Gorgich, H. Mehrbani, and A. Aghakouchakzadeh, "Toward Precision

Diagnosis of Maxillofacial Pathologies by Artificial Intelligence Algorithms: A Systematic Review," *Journal of Maxillofacial and Oral Surgery*, vol. 24, no. 4, pp. 1151–1178, 2025, doi: 10.1007/s12663-025-02664-4.

[9] S. Arzani, A. Karimi, P. Iranmanesh, H. Bang, and P. M. H. Dummer, "Examining the diagnostic accuracy of artificial intelligence for detecting dental caries across imaging modalities: An umbrella review with meta-analysis," *PLoS One*, vol. 20, no. 8, e0329986, 2025, doi: 10.1371/journal.pone. 0329986.

[10] Z. Can and E. Aydin, "Explainable CNN–radiomics fusion and ensemble learning for multimodal lesion classification in dental radiographs," *Diagnostics*, vol. 15, no. 16, p. 1997, 2025, *doi:* 10.3390/diagnostics15161997.

[11] E. Y. Park, H. Cho, S. Kang, and E.-K. Kim, "Caries detection with tooth surface segmentation on intraoral photographic images using deep learning," *BMC Oral Health*, vol. 22, p. 573, 2022, doi: 10.1186/s12903-022-02589-1.

[12] F. Yuce, C. Buyuk, E. Bilgir, Ö. Çelik, and İ. Ş. Bayrakdar, "Deploying a novel deep learning framework for segmentation of specific anatomical structures on cone-beam CT," *Oral Radiology*, vol. 41, no. 4, pp. 562–570, 2025, doi: 10.1007/s11282-025-00831-4.

[13] M. Alahmari *et al.*, "Accuracy of artificial intelligence-based segmentation in maxillofacial structures: A systematic review," *BMC Oral Health*, vol. 25, no. 1, p. 350, 2025. doi: 10.1186/s12903-025-05730-y.

[14] P. Singh and P. Sehgal, "G.V. Black classification of dental caries using CNN," in *Advances in Intelligent Systems and Computing*, Springer, 2021, doi: 10.1007/978-981-15-6584-7_11.

[15] S. Kang, B. Shon, E. Y. Park, and E.-K. Kim, "Diagnostic accuracy of dental caries detection using ensemble techniques in deep learning with intraoral camera images," *PLoS ONE*, vol. 19, no. 8, e03029986, 2024, doi: 10.1371/journal.pone.0310004.

[16] L. Zanini, I. Rubira-Bullen, and F. Nunes, "Enhancing dental caries classification in CBCT images by using image processing and self-supervised learning," *Computers in Biology and Medicine*, vol. 168, 107642, 2024, doi: 10.1016/j.compbiomed.2024. 109221.

[17] H. Shan, Y. Chen, W. Liu, and Q. Zhang, "Semantic-aware synthesis network for dental caries image generation from CBCT to Micro-CT," in *2024 IEEE International Conference on Bioinformatics and Biomedicine (BIBM),* IEEE, Dec. 2024, pp. 2376–2381. doi: 10.1109/BIBM62325.2024.10821817.

[18] J. Rudol, A. Los, B. Lipka, and M. Tysiąc-Miśta, "The use of artificial intelligence in caries detection: Literature review," *Wiadomosci Lekarskie*, vol. 78, no. 1, 2025, doi: 10.36740/WLek/202055.

[19] R. Rathod, S. Dean, and C. Sproat, "The effectiveness of a novel artificial intelligence model in detecting oral and dental diseases," *BDJ Open*, vol. 11, no. 1, p. 62, Jun. 2025, doi: 10.1038/s41405-025-00336-6.

[20] A. Bhan, G. Vyas, S. Mishra, and P. Pandey, "Detection and grading severity of caries in dental X-ray images," in *2016 International Conference on Micro-Electronics and Telecommunication Engineering (ICMETE)*, IEEE, Sep. 2016, pp. 375–378. doi: 10.1109/ICMETE.2016.128.

[21] A. Bhan, A. Goyal, H. Harsh, and C.-W. Wang, "Feature line profile-based automatic detection of dental caries in bitewing radiography," in *2016 International Conference on Micro-Electronics and Telecommunication Engineering (ICMETE)*, IEEE, Sep. 2016, pp. 635–640. doi: 10.1109/ICMETE.2016.59.

[22] A. Hampiholi, V. Kusanur, and B. Sujaya, "Automated dental cavity detection in front teeth using image processing," in *2025 International Conference on Intelligent and Innovative Technologies in Computing, Electrical and Electronics (IITCEE)*, IEEE, Jan. 2025, pp. 1–5. doi: 10.1109/IITCEE64140.2025.10915321.

[23] A. Choudhary, G. Raj, A. P. Agrawal, and D. Bhargava, "An effective approach for classification of dental caries using convolutional neural networks," in *2021 10th International Conference on System Modeling & Advancement in Research Trends (SMART)*, IEEE, Dec. 2021, pp. 204–209. doi: 10.1109/SMART52563.2021.9676250.

[24] S. Kalita, R. C. Singh, A. I. Abidi, and H. Sawhney, "A deep learning based enhanced computational model for dental caries classification," *Proceedings on Engineering Sciences*, vol. 6, no. 2, pp. 115–122, 2024, doi: 10.24874/PES06.02A.001.

[25] M. Moran, M. Faria, G. Giraldi, and A. Conci, "Classification of approximal caries in bitewing radiographs using convolutional neural networks," *Sensors*, vol. 21, no. 12, p.

4154, 2021, doi: 10.3390/s21155192.
[26] P. Nageswari, P. K. Pareek, A. Suresh Kumar, and M. Kandasamy, "A survey analysis on dental caries detection from RVG images using deep learning," in *Lecture Notes in Electrical Engineering*, Springer, 2024, doi: 10.1007/978-981-99-7633-1_12.
[27] Y. Jusman, A. Widyaningrum, W. Tyassari, and E. Saleh, "Classification of caries X-ray images using multilayer perceptron models based on shape features," in*2022 IEEE 7th International Conference on Information Technology and Digital Applications (ICITDA)*, IEEE, Nov. 2022, pp. 1–6. doi: 10.1109/ICITDA55840.2022.9971452.
[28] Y. Jusman, M. K. Anam, S. Puspita, and E. Saleh, "Machine learnings of dental caries images based on Hu moment invariants features," in*2021 International Seminar on Application for Technology of Information and Communication (iSemantic)*, IEEE, Sep. 2021, pp. 296–299. doi: 10.1109/iSemantic52711.2021.9573208.
[29] Y. Jusman, D. N. Aini, S. Puspita, and A. N. N. Chamim, "Caries level classification using combination of Hu and Zernike invariant moments features and machine learning," in *2023 6th International Conference on Information and Communications Technology (ICOIACT)*, IEEE, Nov. 2023, pp. 189–193. doi: 10.1109/ICOIACT59844.2023. 10455798.
[30] Y. Jusman, M. Anam, S. Puspita, E. Saleh, S. Kanafiah, R. Tamarena, "Comparison of dental caries level images classification performance using KNN and SVM methods," in *2021 IEEE International Conference on Signal and Image Processing Applications (ICSIPA)*, IEEE, Sep. 2021, pp. 167–172, doi: 10.1109/ICSIPA52582.2021.9576774.
[31] V. Geetha, K. S. Aprameya, and D. M. Hinduja, "Dental caries diagnosis in digital radiographs using back-propagation neural network," *Health Information Science and Systems*, vol. 8, no. 1, 2020, doi: 10.1007/s13755-019-0096-y.
[32] S. Arora, S. K. Tripathy, R. Gupta, and R. Srivastava, "Exploiting multimodal CNN architecture for automated teeth segmentation on dental panoramic X-ray images," *Proc. IMechE Part H: J. Eng. Med.*, vol. 237, no. 3, pp. 395–405, 2023.
[33] W. Lin, A. Alfaraj, F. Lippert, and C. Yang, "Performance of the caries diagnosis feature of intraoral scanners and near-infrared imaging technology—A narrative review," *Journal of Prosthodontics*, vol. 32, no. S2, pp. 114–124, 2023, doi: 10.1111/jopr.13770.
[34] S. Chung, D. Fried, M. Staninec, and C. L. Darling, "Near infrared imaging of teeth at wavelengths between 1200 and 1600 nm," in *Proceedings of SPIE--the International Society for Optical Engineering*, vol. 7884, pp. 78840H-1–78840H-7, 2011, doi: 10.1117/12.878894.
[35] K. Cuenin, J. Chen, S. K. Tai, and H. Oh, "Caries detection and characterization in pediatric patients using iTero 5D near-infrared technology," *American Journal of Orthodontics and Dentofacial Orthopedics,* vol. 165, no. 1, pp. 56–64, 2024, doi: 10.1016/j.ajodo.2023.06.026.
[36] P. Usenik, M. Bürmen, A. Fidler, and B. Likar, "Improved classification and visualization of healthy and pathological hard dental tissues by modeling specular reflections in NIR hyperspectral images," in *Medical Imaging 2012: Computer-Aided Diagnosis*, SPIE, pp. 84272D-1–84272D-9, 2012, doi: 10.1117/12.911623
[37] H. S. Salehi, M. Mahdian, M. M. Murshid, and A. Tadinada, "Deep learning-based quantitative analysis of dental caries using optical coherence tomography: An ex vivo study," in *Lasers in Dentistry XXV*, SPIE, Feb. 2019, p. 16. doi: 10.1117/12.2510076. doi: 10.1109/ICOIACT59844.2023.10455798.
[38] F. Tetschke, L. Kirsten, J. Golde, and C. Hannig, "Application of optical and spectroscopic technologies for the characterization of carious lesions *in vitro*," *Biomedizinische Technik*, vol. 63, no. 5, pp. 531–540, 2018, doi: https://doi.org/10.1515/bmt-2017-0133.
[39] V. Periyasamy, K. Gisi, and M. Pramanik, "Ex vivo human teeth imaging with various photoacoustic imaging systems," *Biomedical Optics Express*, vol. 15, no. 4, pp. 2211–2225, 2024, doi: 10.1364/BOE.15.002211.
[40] D. P. Popescu, M. G. Sowa, M. D. Hewko, and L.-P. Choo-Smith, "Assessment of early demineralization in teeth using signal attenuation in optical coherence tomography images," *Journal of Biomedical Optics*, vol. 13, no. 5, 054051, 2008, doi: 10.1117/1.3006335.
[41] B. Shi, J. Niu, X. Zhou, and X. Dong, "Quantitative assessment methods of early enamel caries with optical coherence tomography: A review," *Applied Sciences (Switzerland)*, vol. 12, no. 23, 12190, 2022, doi: 10.3390/app122312190.
[42] E. B. Shokouhi, M. Razani, A. Gupta, and N. Tabatabaei, "Comparative study on the

detection of early dental caries using thermo-photonic lock-in imaging and optical coherence tomography," *Biomedical Optics Express*, vol. 9, no. 11, pp. 5310–5324, 2018, doi: 10.1364/BOE.9.005310.

[43] G. Özkan, A. Kanli, N. M. Başeren, and İ. Tatar, "Validation of micro-computed tomography for occlusal caries detection: An *in vitro* study," *Brazilian Oral Research*, vol. 29, no. 1, pp. 1–8, 2015, doi: 10.1590/1807-3107bor-2015.vol29.0132

[44] C. Boca, B. Truyen, L. Henin, and P. Bottenberg, "Comparison of micro-CT imaging and histology for approximal caries detection," *Scientific Reports,* vol. 7, 6683, 2017, doi: 10.1038/s41598-017-07020-2.

[45] R. Welch, K. Sivagurunathan, P. Tavakolian, and A. Mandelis, "Detection of bacteria-induced early-stage dental caries using three-dimensional mid-infrared thermophotonic imaging," *Bioengineering*, vol. 10, no. 6, 675, 2023, doi: 10.3390/bioengineering10060675.

[46] J. Hu, X. Zhang, and Z. Xiong, "Terahertz spectral imaging and gradient-domain fusion for improved detection of dental caries," in *2024 IEEE International Conference on Smart Internet of Things (SmartIoT)*, IEEE, Nov. 2024, pp. 286–292. doi: 10.1109/SmartIoT62235.2024.00051.

[47] J. B. Lazaro, L. J. F. Bitangcor, J. M. A. Dumapit, and J. N. Mapote, "Assistive method for the detection of dental caries using blob spot detection algorithm," in *2024 14th International Conference on Biomedical Engineering and Technology*, ACM, Jun. 2024, pp. 96–100. doi: 10.1145/3678935.3678952.

[48] J. S. Holtzman, D. Kohanchi, J. Biren-Fetz, and P. Wilder-Smith, "Detection and proportion of very early dental caries in independent living older adults," *Lasers in Surgery and Medicine*, vol. 47, no. 7, pp. 584–591, 2015, doi: 10.1002/lsm.22390.

[49] L.-P. Choo-Smith, M. D. Hewko, M. L. Dufour, and M. G. Sowa, "Ex vivo imaging of early dental caries within the interproximal space," in *Lasers in Dentistry XV*, SPIE, Feb. 2009, pp. 71620K-1–71620K-9, doi: 10.1117/12.810435.

[50] S. Yamuna & K.P. Vijayakumar, "Transforming 3D Brain MRI Data: Building a Robust Preprocessing Pipeline," *International Journal of Electronics and Communication Engineering*, *11*(4), 51, 2024, doi: 10.14445/23488549/ijece-v11i4p106

[51] J. Naam, "Accuracy of panoramic dental X-ray imaging in detection of proximal caries with multiple morphological gradient (MMG) method," *International Journal on Informatics Visualization*, vol. 1, no. 1, pp. 18–22, 2017, doi: 10.30630/joiv.1.1.18-22.

[52] V. Majanga and S. Viriri, "Automatic blob detection for dental caries," *Applied Sciences (Switzerland)*, vol. 11, no. 23, 11364, 2021, doi: 10.3390/app112311364.

[53] P. Sehgal, R. Bansal, and P. Singh, "A wavelet-based statistical technique for dental caries severity classification using fuzzy feature selection," *Journal of Theoretical and Applied Information Technology*, vol. 101, no. 4, pp. 569–578, 2023.

[54] L. Zanini, I. Rubira-Bullen, and F. Nunes, "A systematic review on caries detection, classification, and segmentation from X-ray images: Methods, datasets, evaluation, and open opportunities," *Journal of Imaging Informatics in Medicine*, vol. 6, no. 1, pp. 45–60, 2024, doi: 10.1007/s10278-024-01054-5.

[55] S. Patil and S. Nirkhi, "Deep learning techniques for oral diagnosis and cavity recognition: A systematic approach," *International Journal of Advanced Science and Technology*, vol. 29, no. 5, pp. 4982–4991, 2020. doi:

[56] S. V. Kumari and K. U. Rani, "Analysis on various feature extraction methods for medical image classification," in *Advances in Computational and Bio-Engineering*, Springer, 2020, pp. 19–31. doi: 10.1007/978-3-030-46943-6_3.

[57] J. Ge and H. Liu, "Investigation of image classification using HOG, GLCM features, and SVM classifier," in *Man-Machine-Environment System Engineering*, Springer, 2020, pp. 411–417. doi: 10.1007/978-981-15-6978-4_49.

[58] B. Bhattarai, R. Subedi, R. R. Gaire, E. Vazquez, and D. Stoyanov, "Histogram of oriented gradients meet deep learning: A novel multi-task deep network for 2D surgical image semantic segmentation," *Medical Image Analysis*, vol. 85, 2023, doi: 10.1016/j.media.2023.102747.

[59] S. Wang, S. Du, A. Atangana, A. Liu, and Z. Lu, "Application of stationary wavelet entropy in pathological brain detection," *Multimedia Tools and Applications*, vol. 77, no. 3, pp. 3701–3714, 2018, doi: 10.1007/s11042-016-3401-7.

[60] X. Zhou, S. Wang, W. Xu, G. Ji, P. Phillips, P. Sun, and Y. Zhang, "Detection of pathological brain in MRI scanning based on wavelet-

entropy and Naïve Bayes classifier," in *Bioinformatics and Biomedical Engineering*, Springer, 2015, pp. 201–209. doi:10.1007/978-3-319-16483-0_20

[61] L. Zang and Y. Li, "Multi-scale frequency domain learning for texture classification," *International Journal of Machine Learning and Cybernetics*, 2024, doi: 10.1007/s13042-024-02314-0.

[62] M. Goyani and N. Patel, "Template matching and machine learning-based robust facial expression recognition system using multi-level Haar wavelet," *Int. J. Comput. Appl.*, vol. 42, no. 4, pp. 360–371, 2020, doi: 10.1080/1206212X.2017.1395134.

[63] D. Anggoro and D. Permatasari, "Performance comparison of the kernels of support vector machine algorithm for diabetes mellitus classification,"*International Journal of Advanced Computer Science and Applications*, vol. 14, no. 1, pp. 580–585, 2023, doi: 10.14569/IJACSA.2023.0140163.

[64] S. Malik, A. Mire, A. K. Tyagi, and V. Arora, "A novel feature extractor based on the modified approach of histogram of oriented gradient," in *Computational Science and Its Applications – ICCSA 2020*, Springer, 2020, pp. 753–770. doi: 10.1007/978-3-030-58817-5_54.

[65] S. V. Kumari and K. U. Rani, "Analysis on various feature extraction methods for medical image classification," in *Advances in Computational and Bio-Engineering*, Springer, 2020, pp. 19–31.

[66] B. Abhisheka, S. Kr, and B. Biswajit, "HBMD-Net: Feature fusion based breast cancer classification with class imbalance resolution,"*Journal of Imaging Informatics in Medicine*, vol. 37, no. 4, pp. 1440–1457, 2024, doi: 10.1007/s10278-024-01046-5.

[67] S. Lee, S.-I. Oh, J. Jo, S. Kang, Y. Shin, and J.-W. Park, "Deep learning for early dental caries detection in bitewing radiographs," *Scientific Reports*, vol. 11, 16807, 2021, doi: 10.1038/s41598-021-96368-7.